ELSEVIER

International Journal of Fatigue 21 (1999) 653–662

International Journal of Fatigue

www.elsevier.com/locate/ijfatigue

Thresholds for high-cycle fatigue in a turbine engine Ti–6Al–4V alloy

R.O. Ritchie [a,*], B.L. Boyce [a], J.P. Campbell [a], O. Roder [a], A.W. Thompson [a], W.W. Milligan [b]

[a] *Department of Materials Science and Mineral Engineering, University of California, Berkeley, CA 94720-1760, USA*
[b] *Department of Metallurgical and Materials Engineering, Michigan Technological University, Houghton, MI 49931-0001, USA*

Received 1 June 1998; received in revised form 1 December 1998

Abstract

The characterization of critical levels of microstructural damage that can lead to fatigue-crack propagation under high-cycle fatigue loading conditions is a major concern for the aircraft industry with respect to the structural integrity of turbine engine components. The extremely high cyclic frequencies characteristic of in-flight loading spectra necessitate that a damage-tolerant design approach be based on a crack-propagation threshold, ΔK_{TH}. The present study identifies a practical lower-bound large-crack threshold under high-cycle fatigue conditions in a Ti–6Al–4V blade alloy (with ~60% primary α in a matrix of lamellar $\alpha+\beta$). Lower-bound thresholds are measured by modifying standard large-crack propagation tests to simulate small-crack behavior. These techniques include high load-ratio testing under both constant-R and constant-K_{max} conditions, performed at cyclic loading frequencies up to 1 kHz and R-ratios up to 0.92. The results of these tests are compared to the near-threshold behavior of naturally-initiated small cracks, and to the crack initiation and early growth behavior of small cracks emanating from sites of simulated foreign object damage.

Keywords: Fatigue; Threshold; Titanium; High-cycle fatigue small cracks; Foreign object damage

1. Introduction

A 1992 study conducted by the Scientific Advisory Board of the US Air Force targeted high-cycle fatigue (HCF) as the single biggest cause of turbine engine failures in military aircraft [1]. HCF results in rapid, essentially unpredictable failures due to fatigue-crack propagation under ultrahigh frequency loading. Furthermore, cracking often initiates from small defects which are associated with damage caused by a variety of drivers, including fretting and impacts by foreign objects [2]. To prevent HCF failures, design methodologies are required that identify the critical levels of precursory microstructural damage which can lead to such failure. The current study, which is part of the US Air Force's Multidisciplinary University Research Initiative on 'High Cycle Fatigue,' is targeted at identifying these critical levels of damage and characterizing fatigue behavior under representative operating conditions in a Ti–6Al–4V alloy. The Ti–6Al–4V alloy, typically used in the front, low-temperature, stages of the engine, was chosen as a prototypical material for study by the joint military–industry–academia HCF program.

While the exact forcing functions which cause HCF failure remain unknown, it has been established that engine components experience high frequency (>1 kHz) vibrational loading due to transient airflow dynamics [2, 3]. This vibratory loading is often superimposed on a high mean stress. Because of the very high frequency of loading, even cracks growing at slow per-cycle velocities (i.e. 10^{-10} to 10^{-9} m/cycle) propagate to failure in a short period of time. For example, a crack growing at a constant velocity of 10^{-10} m/cycle would cause failure in a 20 mm thick turbine component in approximately 30 h of operation (at 1 kHz). In contrast, this same crack velocity in a 20 mm automobile piston rod would give 2000 h of continuous operation due to the low frequency of loading (~50 Hz). For this reason, it is necessary to

* Corresponding author. Tel: (510)486-5798; fax: (510)486-4995.
E-mail address: roritchie@lbl.gov (R.O. Ritchie)

0142-1123/99/$ - see front matter.
PII: S0142-1123(99)00024-9

operate HCF-critical turbine components below the fatigue-crack propagation threshold (ΔK_{TH}) such that crack propagation cannot occur (within ~10^9 cycles).

Whereas an extensive database [4,5] exists for fatigue-crack propagation thresholds in metallic alloys, it has been largely derived from standard test geometries containing large (>few mm) through-thickness cracks; such data are not necessarily relevant to the HCF problem where the flaws that cause failure are likely to be in the range of tens to hundred of micrometers [6]. Indeed, cracks with dimensions comparable to either characteristic microstructural size scales or to the crack-tip plastic-zone size can grow at velocities far faster than corresponding large cracks at the same *applied* driving force; and they can propagate at applied stress-intensity levels *below* the large-crack threshold, ΔK_{TH} (Fig. 1). For this reason, design against HCF failure must be based on the notion of a small-crack threshold, measured under the representative conditions of high frequencies and high mean loads [7].

There are several reasons why small cracks can behave differently from large-cracks. Of these, the most important are associated with cracks of a size comparable to [8]:

- microstructural size scales, where biased statistical sampling of the microstructure leads to accelerated crack advance along 'weak' paths, i.e., microstructural features oriented for easy crack growth (a continuum or homogeneity limitation),
- the extent of local plasticity *ahead* of the crack tip, where the assumption of small-scale yielding implicit in the use of the stress intensity K is not strictly valid (a linear-elastic fracture mechanics limitation),
- the extent of crack-tip shielding (e.g. crack wedging by crack closure) *behind* the crack tip, where the reduced role of shielding leads to a higher *local* driving force than the corresponding large crack at the same K levels (a similitude limitation).

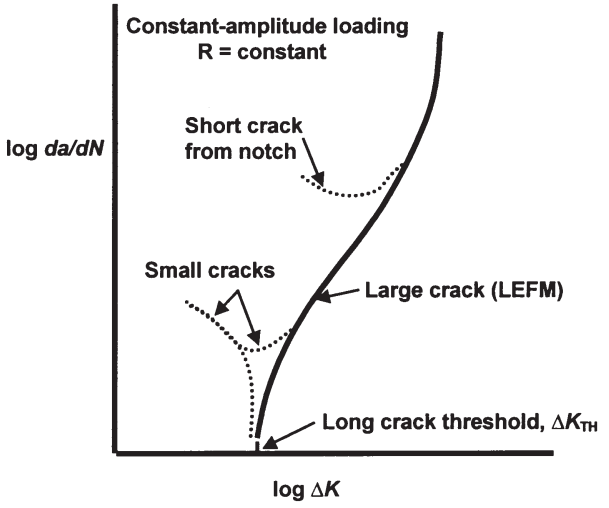

Fig. 1. A schematic comparison of typical growth-rate behavior for small cracks and large cracks. Small cracks are observed to grow below the large-crack threshold and at velocities greater than equivalently driven large cracks.

Because of the experimental difficulties associated with conducting small-crack tests, one approach used in the present work is to develop, through a consideration of the mechanisms listed above, large-crack tests that simulate the behavior of small cracks, thereby yielding *lower-bound* threshold values. As small-scale yielding conditions, in terms of near-threshold cyclic plastic-zone sizes (~0.2–1 μm), clearly apply, the methods of determining lower-bound thresholds used in this study are focused on the similitude limitation, and are thus based on assuring that (i) minimal crack closure exists *behind* the crack tip, and (ii) minimal microstructural damage exists *ahead* of the tip. We recognize that such lower-bound large-crack techniques cannot also simulate the continuum limitation; however, the extent to which they do simulate true small-crack behavior will give some insight into the importance of this factor.

The techniques being employed are:

- conventional load-shedding to approach the threshold under high and *constant* load-ratio conditions [Fig. 2(a)], where the load ratio R is the ratio of minimum to maximum loads; this tends to minimize the role of crack closure by ensuring that crack-tip opening displacements (CTODs) are large enough to limit any premature contact of the crack surfaces on unloading (i.e. the minimum CTOD in the cycle is larger than the dimensions of the fracture surface asperities),
- load-shedding under variable R conditions, specifically involving a constant K_{max}/increasing K_{min} sequence to approach the threshold [9,10] [Fig. 2(b)], which ensures that the highest R values possible, and hence minimal closure loads, are achieved at ΔK_{TH},
- pre-cracking in far-field compression to minimize microstructural damage ahead of the crack tip [6,11,12], followed by machining to remove the crack wake,
- 'razor micro-notching', where polishing with a razor blade at the root of a notch is used to produce a machined slot (i.e. with no crack closure and little damage ahead of the tip) with a root radius smaller than the characteristic microstructural dimensions (~10 μm).

The current paper describes results using the first two techniques. In addition, as many engine components see the high frequency/high load-ratio (vibratory) cycling interrupted by large periodic unloading/loading (stop–start) cycles, we take a preliminary look at this effect of high-cycle/low-cycle fatigue (HCF/LCF) interactions on such thresholds. A secondary objective is to investigate

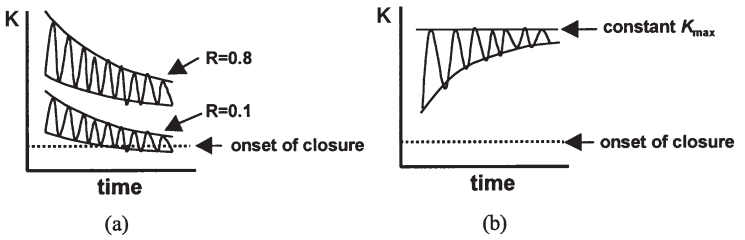

Fig. 2. Schematics illustrating the use of (a) high load ratio and (b) constant K_{max} cycling to minimize closure effects, thereby yielding lower-bound thresholds.

the effect of frequency on crack-growth behavior in Ti–6Al–4V; as many of the HCF data are measured at 1 kHz, comparisons are made with results at 'conventional' frequencies (e.g. 50 Hz). Finally, since foreign object damage represents a prime source of HCF failures, we also examine the fatigue-crack growth behavior of small cracks originating from foreign object damage sites that have been simulated by firing high-velocity hardened steel spheres onto the surface of test samples.

2. Experimental procedures

2.1. Material and microstructure

The Ti–6Al–4V alloy investigated in this study was supplied in a condition which has been termed 'solution-treated and overaged' (STOA), from a set of forgings produced specifically for the joint military–industry–academia HCF program. The chemical composition (in wt%) was 6.30% Al, 4.17% V, 0.19% Fe, 0.19% O, 0.013% N, bal. Ti. The bar-stock, originating from Teledyne Titanium, was forged into 40×15×2 cm plates and subsequently solution-treated at 925°C (1 h) and vacuum annealed at 700°C (2 h) for stabilization. The resulting microstructure consisted of a bimodal distribution of ~60 vol% primary-α and ~40 vol% lamellar colonies of α+β (Fig. 3). Studies of a separate forging from the same lot revealed a tensile strength of 970 MPa, a yield strength of 926–935 MPa and a Young's modulus of 116 GPa, based on tensile tests conducted along the longitudinal axis at a strain rate of 5×10^{-4} s^{-1} [13].

2.2. Fatigue-crack propagation testing

Large-crack propagation studies were conducted on compact-tension C(T) specimens machined in the L–T orientation (with 8 mm thickness and 25 mm width) at R ratios (ratio of minimum to maximum loads) varying from 0.1 to 0.92 in a lab air environment (22°C, ~45% relative humidity). Crack lengths were monitored in situ using the back-face strain compliance technique, and were verified using periodic optical inspection. Crack closure was also monitored using back-face strain compliance; specifically, the closure stress intensity, K_{cl}, was

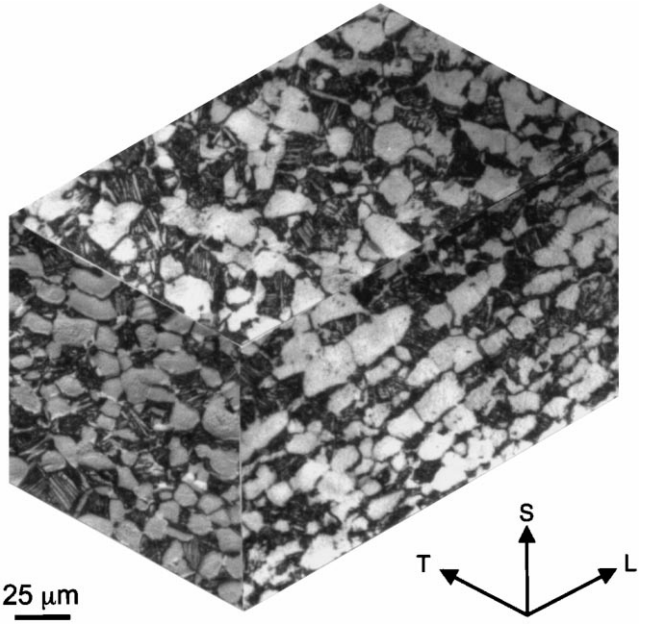

Fig. 3. Optical micrograph of the microstructure of the Ti–6Al–4V studied. The microstructure consists of approximately 60% primary α and 40% lamellar α+β colonies. The grains were slightly elongated in along the L forging axis. All fatigue specimens were extracted in the L–T orientation (such that the crack surface was in the S–T plane and the crack propagated in the T direction). (Etched in Kroll's solution).

determined from the closure load, P_{cl}, measured at the point of first deviation from linearity in the elastic compliance curve upon unloading [14].

Fatigue tests were conducted largely in accordance with ASTM Standard E-647. For crack-growth threshold determination using constant R testing, loads were shed such that $\Delta K=\Delta K_{initial}\exp[C(a-a_{initial})]$, with the normalized K-gradient, C, set to -0.08 mm^{-1}, as suggested in ASTM E-647 (ΔK is the stress-intensity range and a is the crack length).[1] At 50–200 Hz, the fatigue thresholds, ΔK_{TH} and $K_{max,TH}$, were defined as the minimum values of these parameters yielding a propagation rate

[1] Proprietary studies by industrial participants have found that gradients as high as $C=-0.8$ mm^{-1} could be employed for this alloy without inducing observable effects on the measurement of the threshold.

of 10^{-10} m/cycle; at 1 kHz, thresholds could be defined at a propagation rate of 10^{-11} m/cycle.

Tests at 50–200 Hz (sine wave) were conducted on conventional MTS servo-hydraulic testing machines operating under automated closed-loop K control. Corresponding fatigue tests at 1 kHz were performed under load control on a newly developed MTS servohydraulic test frame using a voice-coil servovalve; details of this instrument are described elsewhere [15].

Results are presented in the form of the crack growth increment per cycle, da/dN, plotted as a function of the applied stress-intensity range, $\Delta K=K_{max}-K_{min}$; after allowing for the effect of closure, growth rates are plotted as a function of the effective (near-tip) stress-intensity range, $\Delta K_{eff}=K_{max}-K_{cl}$.

2.3. Simulation of foreign object damage

Foreign object damage (FOD) was simulated by firing chrome-hardened steel spheres onto a flat specimen surface using compressed gas. The specimen geometry chosen for this study has a rectangular gauge section with cylindrical buttonhead grip sections (Fig. 4), and is nearly identical to the K_b specimen used by GE Aircraft Engines for its similarity to the blade loading configuration [16]. To provide a consistent, nominally stress-free surface, gauge sections were prepared by standard stress relief and chemical-milling procedures. In this study, 3.2 mm diameter spheres were impacted onto the flat surface of a tensile specimen at velocities of ~200, 250, and 300 m/s. These velocities were chosen because (i) they represented typical in-service impact velocities on blades, and (ii) they provided different levels of damage (see below). All shots were fired at 90° to the specimen surface. After impacting, the tensile specimens were subsequently cycled at 20 Hz (sine wave) with a maximum nominal stress of 500 MPa at a load ratio of R=0.1. Periodically, the specimen was removed from the test frame and examined in a scanning electron microscope (SEM) to detect crack initiation. Once a crack had initiated, subsequent crack growth was similarly monitored using periodic SEM observations. As a preliminary assessment, residual stresses surrounding the indentation were ignored and the fatigue cracks were modeled as semi-elliptical surface cracks initiating at the bottom or rim of the impact crater. Stress intensities were computed from the Newman–Raju semi-elliptical surface crack solution [17], assuming a half-surface length to depth ratio (c/a) of 0.9 (based on fractographic observations).

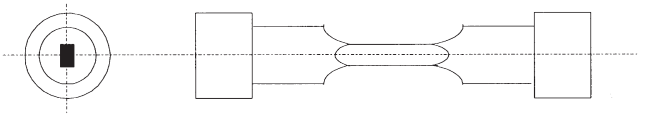

Fig. 4. Modified K_b geometry used for FOD studies. Gauge section is 3 mm × 5 mm. The specimen is based on a geometry used by General Electric to closely approximate the loading configuration of actual turbine blades. The FOD shot was fired at the 5 mm wide surface and created impact sites that were 2–2.6 mm in diameter.

3. Results and discussion

3.1. Effect of load ratio

The effect of load ratio (R=0.1–0.8) on the fatigue-crack propagation rates of large (>5 mm) cracks in the STOA Ti–6Al–4V at low frequencies (50 Hz) is shown in Fig. 5. As expected, higher load ratios induce lower ΔK_{TH} thresholds and faster growth rates at a given applied ΔK level. Threshold stress-intensity ranges were measured as 4.6, 2.9, and 2.6 MPa√m at R=0.1, 0.5 and 0.8, respectively. A two-parameter fit of the Paris regime for the three load ratios yields a growth law of (units: m/cycle, MPa√m):

$$\frac{da}{dN}=5.2\times10^{-12}\Delta K^{2.5}K_{max}^{0.67} \quad (1)$$

While this law appears to work well at both of the higher load ratios, at R=0.1 there is clearly a slight transition in slope at ΔK~10 MPa√m that cannot be captured in Eq. (1). This transition has been observed in similar Ti–6Al–4V alloys and has been attributed to a change in the crystallographic morphology of crack growth, from a 'stage-I like' fracture where all facets lie on the basal plane (0002) to a typical stage-II transgranular fracture resulting from slip alternating on nearly symmetrical slip systems [18].

The observed effect of load ratio is commonly attri-

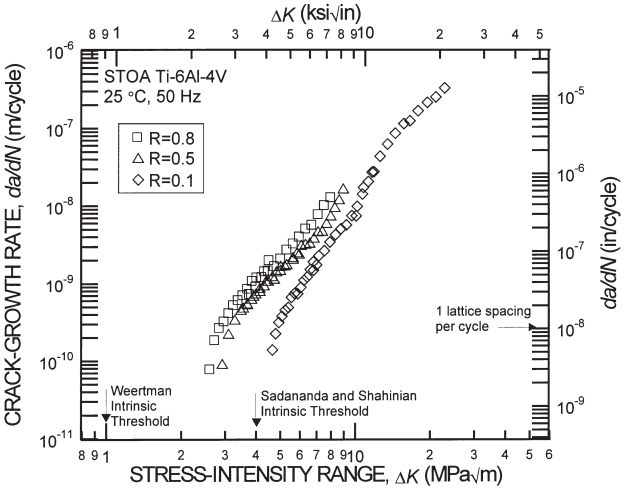

Fig. 5. Fatigue crack propagation data for R=0.1, 0.5, and 0.8 with thresholds at ΔK_{TH}=4.6, 2.9, and 2.6 MPa√m, respectively. Thresholds are compared to theoretical intrinsic thresholds based on analysis by Weertman [29], and Sadananda and Shahinian [28], as discussed in the text.

buted to the role of crack closure, which in Ti alloys is generally observed to be roughness induced (i.e. arising from the wedging of crack-surface asperities) [19–21]. To examine this, closure stress intensity values, K_{cl}, were measured at each load ratio. No detectable closure was observed at R=0.5 and 0.8. However, at R=0.1, K_{cl} values were observed to be roughly constant at ~2.0 MPa√m [Fig. 6(a)]. In Fig. 6(b), the results of Fig. 5 are replotted in terms of the effective stress-intensity range, after accounting for crack closure. It is apparent that, similar to previous studies in Ti–6Al–4V [22], characterizing growth rates in terms of ΔK_{eff} reduces the disparity in crack-growth behavior between the three R ratios; this result is consistent with crack closure as a mechanism for the load ratio (or K_{max}) effect.

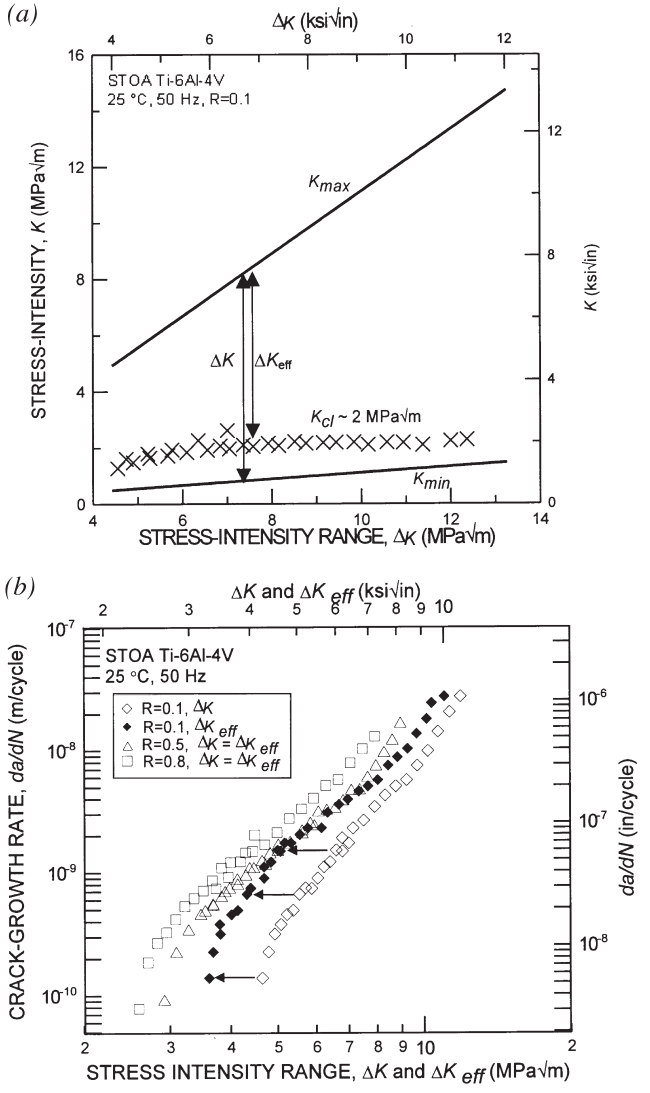

Fig. 6. (a) Crack closure, measured by unloading compliance, stays approximately constant at K_{cl}~2 MPa√m. (b) When crack closure is considered in ΔK_{eff} (=$K_{max}-K_{cl}$), the load ratio effect between R=0.1 and R=0.5 is negligible. At low growth rates, the apparent discrepancy is most likely due to imprecision in measuring the closure level.

The measured variation with load ratio of the threshold ΔK_{TH} and $K_{max,TH}$ values, plotted in Fig. 7, can be compared with the simple closure model of Schmidt and Paris [24]. This model is based on the notion that K_{cl} and the effective ΔK threshold, $\Delta K_{eff,TH}$, are constant and independent of R; it predicts that measured ΔK_{TH} and $K_{max,TH}$ thresholds will be load-ratio independent, respectively above and below a transition R at which point $K_{min}=K_{cl}$. Although clearly there are insufficient data to verify this simplified analysis, the present results

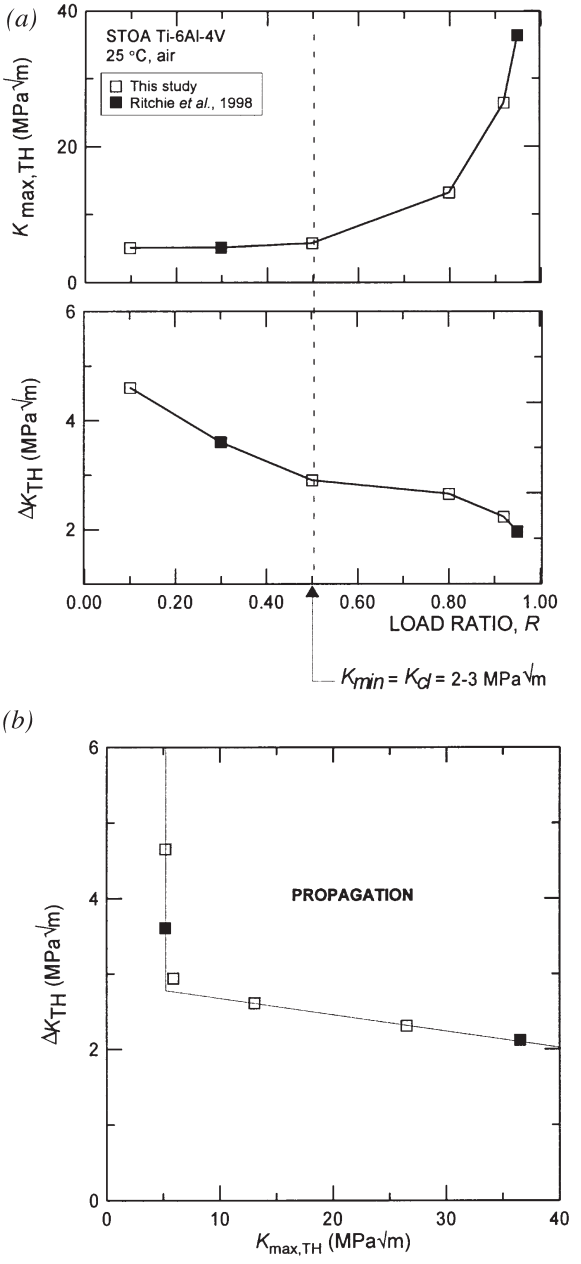

Fig. 7. Variation of $K_{max,TH}$ and ΔK_{TH} with load ratio appears to follow the Schmidt and Paris closure model [23]. Although more data are required to clearly establish a transition, the data presented here show a change in slope at R≈0.5, consistent with K_{cl}=2–3 MPa√m as observed.

are consistent with this model, and the transition R, above which closure is ineffective ($K_{min} > K_{cl}$), is observed at $K_{min}=K_{cl} \approx 2$–3 MPa√m. Such an estimate of K_{cl} is consistent with the experimentally measured values [Fig. 6(a)], determined from back-face strain compliance.

3.2. Effect of frequency

The role of cyclic frequency is shown in Fig. 8 where the growth rates at 50 Hz are compared with data collected at 1 kHz. It is clear that results at 1 kHz are not statistically distinguishable from the conventional frequency data. Cursory experiments performed at 200 Hz exhibited a similar result. This lack of a frequency effect on ambient-temperature *growth-rate* behavior in STOA Ti–6Al–4V is consistent with preliminary results at 2 kHz on the same material system [25]. In contrast, *stress/life* (S/N) fatigue tests conducted in another Ti–6Al–4V microstructure (consisting almost entirely of primary α) [26] showed an increase in fatigue strength (defined as the stress for failure within 10^7 cycles) as the frequency increased from 70 to 400 to 1800 Hz. These results suggest that the role of high frequencies on the fatigue of Ti–6Al–4V at ambient temperatures may be largely associated with crack initiation, rather than the propagation life per se.

Testing at 1 kHz permits thresholds to be readily obtained at much lower growth rates. Using the ASTM standard K-gradient of 0.08 mm^{-1}, measurements down to 10^{-11} m/cycle require several weeks at 50 Hz, whereas these same measurements can be obtained in a single day at 1 kHz. In the present study, thresholds measured at 10^{-11} m/cycle (at 1 kHz) were found to be ~0.1 MPa√m lower than the 10^{-10} m/cycle thresholds (measured at either frequency).

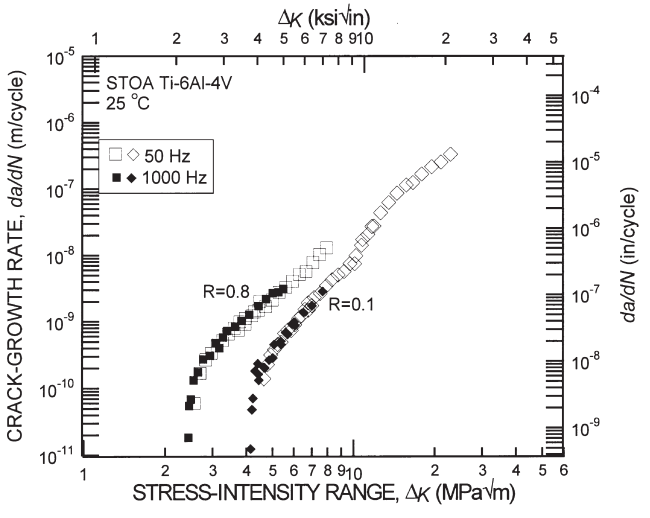

Fig. 8. Comparison of fatigue-crack propagation at 50 Hz and 1 kHz showing no statistically significant deviation in behavior. High frequency testing also enables collection of very low growth rate data (down to 10^{-11} m/cycle) in a relatively short amount of time (~1 day).

3.3. Constant K_{max}/variable R testing

Results at 1 kHz from the variable R, constant-K_{max}/increasing-K_{min} tests, which minimize the effect of crack closure, are shown in Fig. 9. Here, for a constant K_{max} of 26.5 MPa√m, a final load ratio of R=0.92 was achieved, yielding a threshold of 2.2 MPa√m, compared to a ΔK_{TH} value of 2.4 MPa√m for constant R=0.8 testing. These high load ratios result in an extremely large minimum crack-tip opening displacements[2] ($CTOD_{min} \approx 0.7$ μm and 4.3 μm for R=0.8 and 0.92, respectively) superimposed on a relatively small cyclic crack-tip opening displacement ($\Delta CTOD \approx 20$ nm for both R=0.8 and 0.92). With such large crack-tip opening displacements, crack closure from fracture-surface asperity wedging would be expected to be essentially non-existent, as the asperity sizes would need to exceed the $CTOD_{min}$ of several micrometers.

The ΔK_{TH} threshold value of 2.2 MPa√m measured under constant-K_{max}/increasing K_{min} cycling at R=0.92 is considered to represent a practical lower-bound threshold for large cracks measured to date in STOA Ti–6Al–4V. It should be compared with measurements on naturally-initiated small cracks in the same microstructure, where small-crack growth (a~45–1000 μm) was not observed below a ΔK of 2.9 MPa√m (R=0.1) [28].

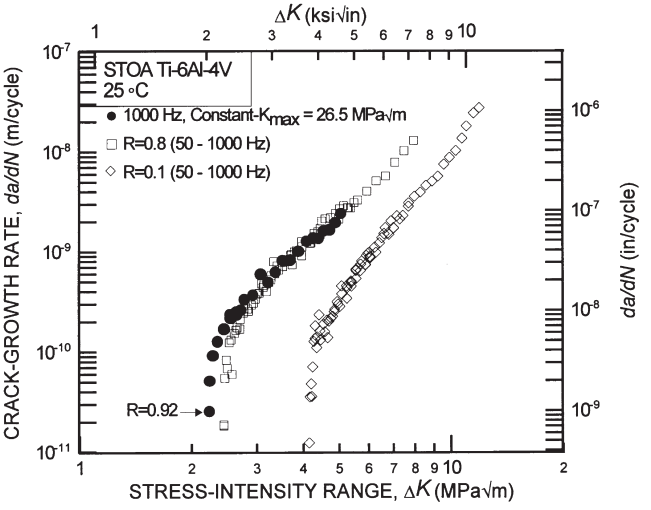

Fig. 9. A constant K_{max} test at 1000 Hz was used to achieve R=0.92 resulting in a lower-bound threshold of 2.2 MPa√m. Results are compared with constant R data at both 50 and 1000 Hz.

[2] Crack-tip opening displacements, δ, were calculated in terms of the yield stress, σ_y, and appropriate Young's modulus, E', from $\delta \approx \beta(K^2/\sigma_y E')$. The constant β is a function of the yield strain, σ_y/E', the strain-hardening coefficient and whether plane-stress or plane-strain conditions are assumed; a value of 0.8 was used for Ti–6Al–4V, based on the numerical calculations of Shih [27].

3.4. Intrinsic thresholds

Since threshold values are experimentally measured at such high load ratios in the apparent total absence of an influence of crack closure, their magnitude should approach that of the so-called *intrinsic* threshold. Several estimates of this parameter have been theoretically calculated to represent the absolute lower-bound stress intensity for fatigue-crack growth.

The simplest approach to estimate the intrinsic threshold is to extrapolate the Paris law regime down to the point where the crack increment per cycle is on the order of a lattice spacing per cycle. In Ti–6Al–4V, this gives lower-bound ΔK_{TH} thresholds of ~4.6 3.0, and 2.8 MPa$\sqrt{m}$ at R values of 0.1, 0.5, and 0.8, respectively. Clearly, this approach is overly simplistic because near-threshold crack advance does not occur uniformly across the entire crack front; the measured da/dN values do not describe growth locally, but rather an average growth occurring over the entire crack front.

A more sound approach is to model the intrinsic threshold in terms of the applied driving force below which dislocations can no longer be emitted from the crack tip [29, 30]. In this regard, the approach of Sadananda and Shahinian [29] considers the total energy required to drive a dislocation from a crack tip as the sum of four components: the 'self' energy of the dislocation, U_s, the surface energy created by the slip step at the crack tip, U_γ, the lattice frictional energy required to move a dislocation, U_f, and the energy from an image force, U_I, imparted by the presence of the nearby free surface (crack wake). This total energy U_T is then converted into a required shear stress and stress intensity:

$$U_T = U_s + U_\gamma + U_f + U_I = \tau_{xy} b^2 \tag{2}$$
$$= \frac{Kb^2}{\sqrt{2\pi\rho}}\left(\cos\frac{\theta}{2}\sin\frac{\theta}{2}\cos\frac{3\theta}{2}\right)$$

where b is the Burgers vector, ρ is the distance between the dislocation and the crack tip (taken here to equal b), θ is the angle between the actual crack propagation direction and the pure Mode-I direction, τ_{xy} is the shear stress required to drive the dislocation, and K is the corresponding stress intensity. The analysis predicts the threshold to occur when K_{max} is no longer sufficient to emit a dislocation, i.e. when:

$$K_{max,TH} \propto \tau_{xy}(b)^{\frac{1}{2}} \tag{3}$$

For Ti–6Al–4V, the predicted intrinsic threshold $K_{max,TH}$ is 4.3 MPa$\sqrt{m}$ *for all R values*. This compares well to the experimentally measured values at R=0.1 where $K_{max,TH}$=5.1 MPa$\sqrt{m}$; however, at R=0.92 where $K_{max,TH}$ is held at 26.5 MPa$\sqrt{m}$, the prediction is clearly questionable, possibly because the analysis is essentially based on static (monotonic) loading and makes no allowance for reversed plasticity and enhanced crack-tip blunting at high R values.

The corresponding approach of Weertman [30] is also based on the limiting conditions for dislocation emission from an atomically sharp crack, in this case using the perfectly brittle Griffith solution modified by a parameter, g, which describes the degree of ductility:

$$\Delta K_{TH} = 2g\left[\frac{2E\gamma}{1-\nu^2}\right]^{\frac{1}{2}} \tag{4}$$

Here E is the Young's modulus, ν is Poisson's ratio, and γ is the true surface energy of the solid. The modifying parameter, g, is a function of the theoretical tensile strength normalized by the theoretical shear strength (typical values are taken between 0.6 and 1, with unity representing the perfectly brittle case). Using this approach, the intrinsic threshold for Ti–6Al–4V is predicted to be on the order of 1 MPa$\sqrt{m}$. Whereas this represents a better estimate of a theoretical lower bound for the fatigue threshold, it is a factor of 2 smaller than experimentally measured lower-bound values, possibly because the approach also does not taken into account cyclic plasticity, both in the form of crack-tip blunting and dislocation shielding arising from the presence of the plastic zone at the crack tip.

3.5. Effect of foreign object damage

As foreign object damage can be a prime source of cracks initiated in HCF, the role of simulated FOD on thresholds and early crack growth was examined using specimens previously impacted by steel shot at velocities between 200 and 300 m/s. An SEM micrograph of a typical impact site at 300 m/s is presented in Fig. 10 with a schematic illustration of the relevant features in the crater profile. While at 300 and 250 m/s, shear bands were seen emanating from the surface of the crater, such shear bands were not observed for 200 m/s impacts. In addition, the 300 m/s impact caused a piling-up of material along the crater rim; this feature was not seen for the lower velocity impacts.

The effect of these impact damage sites was to reduce the fatigue life markedly compared to that obtained with an un-impacted smooth-bar sample. At a maximum applied stress of 500 MPa (R=0.1), single fatigue cracks in the 200 m/s impacted samples were initiated near the bottom of the crater within ~4.3×10^4 cycles, whereas in the 300 m/s FOD site, the crack initiated at the crater rim within ~2.9×10^4 cycles. In terms of total life, the 200 m/s impacted sample also resulted in a longer overall fatigue life of 7.5×10^4 cycles, compared to 4.6×10^4 cycles from the 300 m/s impacted sample. These lives are to be compared with corresponding behavior in a smooth bar, where initiation and total lives at this stress exceed 10^7 cycles (i.e. 500 MPa is below the 10^7-cycle fatigue limit for this material).

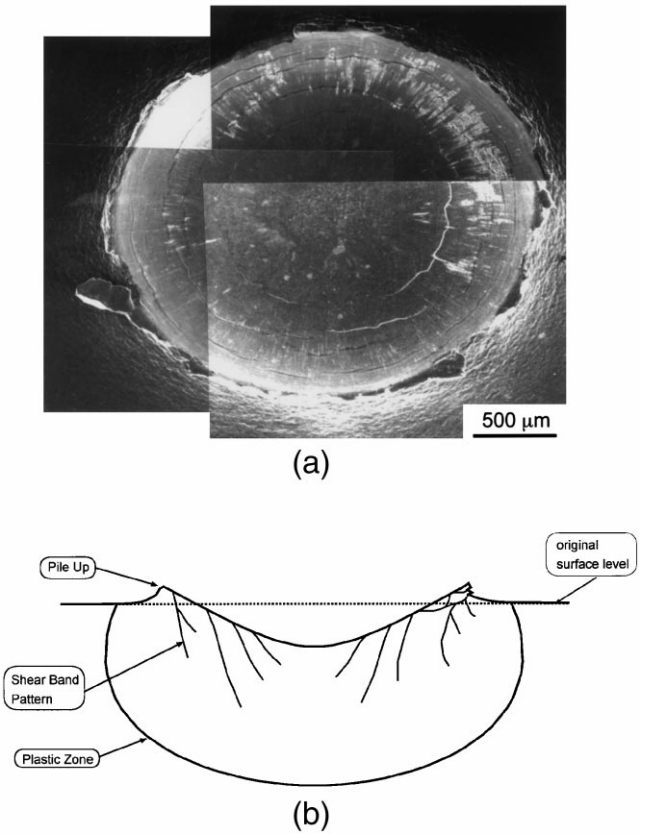

Fig. 10. (a) SEM micrograph of simulated foreign object damage resulting from an impact by a hardened steel sphere with an incident velocity of 300 m/s and (b) corresponding schematic illustrating features present at 300 and 250 m/s. At 200 m/s neither the shear bands nor the 'pile up' were observed.

Consistent with previous low-cycle fatigue results [31], the presence of the shear bands did not appear to play a significant role in the overall fatigue life, e.g. the initiation of the fatigue cracks at damage sites did not appear to be directly associated with them. It is possible, though, that shear banding will have an effect on fatigue behavior at lower applied stresses when lives exceed ~10^6 cycles.

The growth rates of the small cracks originating from such impact sites are compared in Fig. 11 with growth-rate data for large (>5 mm) and naturally-initiated small (~45–1000 μm) cracks in this microstructure. Both the naturally-initiated and FOD-initiated small-crack velocities were within the same scatter band, initially up to an order of magnitude faster than corresponding large-crack results (although small-crack data tended to merge with large-crack results above ΔK = ~10 MPa√m as the crack size increased). However, in the limited data collected to date, no FOD-initiated cracks have been observed in the STOA Ti–6Al–4V material below a ΔK of ~2.9 MPa√m; i.e. no FOD-initiated cracking was observed below the lower-bound (large-crack) threshold, ΔK_{TH}.

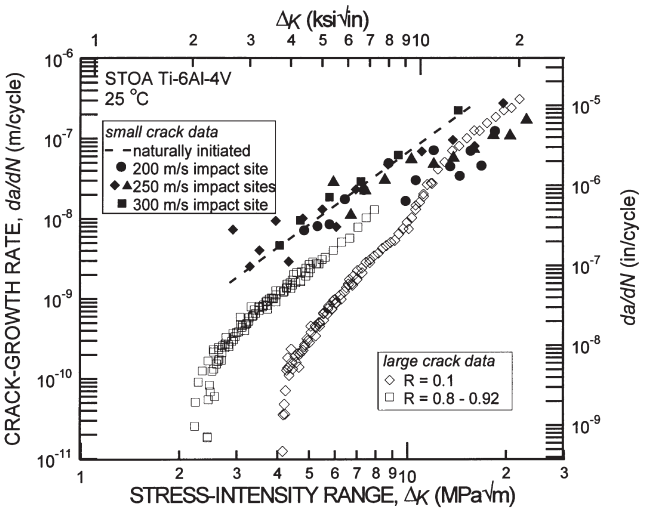

Fig. 11. Fatigue crack propagation rates of naturally-initiated small (45–1000 μm) cracks (dashed line) and small cracks emanating from a variety of FOD impact sites (closed symbols). These small crack results obtained at R=0.1 are compared to large cracks at R=0.1 and R=0.8–0.92 (open symbols).

4. Summary

The problem of turbine engine high-cycle fatigue requires that design must be based on the notion of a threshold stress intensity for no crack growth under the appropriate conditions of high mean loads, ultrahigh frequency (vibratory) loading, and small crack sizes. Since the measurement of small-crack thresholds is experimentally tedious and complex, the approach used in the current work has been to simulate such thresholds with *lower-bound* large-crack measurements. Our preliminary results in Ti–6Al–4V show that using constant K_{max}/increasing K_{min} cycling, a ΔK_{TH} threshold for large (>5 mm) cracks can be measured at very high load ratios (R~0.92) and frequencies (1 kHz) which is a lower bound compared to that of naturally-initiated small (45–1000 μm) cracks and small cracks emanating from sites of foreign object damage.

5. Conclusions

Based on a preliminary investigation into the high-cycle fatigue of a solution treated and overaged Ti–6Al–4V turbine engine alloy, the following conclusions can be made:

1. Ambient-temperature fatigue-crack propagation (over the range ~10^{-11} to 10^{-6} m/cycle) and threshold ΔK_{TH} values were found to be independent of test frequency (50–1000 Hz) for large (>5 mm) through-thickness cracks.
2. A *lower-bound* threshold, measured for large cracks at R=0.92 under constant-K_{max}/increasing-K_{min} con-

ditions, was found to be 2.2 MPa√m for this alloy. This should be compared with measurements on naturally-initiated small cracks and FOD-initiated small cracks in the same microstructure, where small-crack growth was not reported below a ΔK of 2.9 MPa√m.

3. Foreign object damage, simulated by hardened steel spheres impacted at 200–300 m/s on a flat surface, provide sites for the initiation of small fatigue cracks. At applied stresses some 10% below the smooth-bar, 10^7-cycles fatigue strength, crack-initiation lives were less than 4×10^4 cycles, many orders of magnitude shorter than in un-impacted samples. Subsequent small-crack growth from the damage sites was found to occur at rates considerably faster than large cracks subjected to the same applied ΔK level. No crack growth from FOD sites has been observed to date at ΔK values less than 2.9 MPa√m; i.e. no FOD-initiated cracking was seen below the lower-bound ΔK_{TH}.

Acknowledgements

This work was supported by the US Air Force Office of Scientific Research under Grant No. F49620-96-1-0478 under the auspices of the Multidisciplinary University Research Initiative on *High Cycle Fatigue* to the University of California at Berkeley. B.L.B. would also like to acknowledge the support of the Hertz Foundation. Special thanks are due to Prof. G. Lütjering, Dr J.A. Hines and Dr J.O. Peters of the Technische Universität Hamburg-Harburg for providing us with their naturally-initiated small-crack results, and to Dr D.L. Davidson of the Southwest Research Institute for numerous helpful discussions.

References

[1] Report of the AdHoc Committee on Air Force Aircraft Jet Engine Manufacturing and Production Processes. The Pentagon, Washington (DC): United States Air Force Scientific Advisory Board, SAF/AQQS, 1992.
[2] Cowles BA. High cycle fatigue in aircraft gas turbines—an industry perspective. Int J Fract 1996;80:147–63.
[3] Chang JCI. An integrated research approach to attack engine HCF problems. Washington (DC): Air Force Office of Scientific Research, 1996.
[4] Taylor D. A compendium of fatigue thresholds and crack growth rates. Warley (UK): EMAS Ltd, 1985.
[5] Ritchie RO. Near-threshold fatigue crack propagation in steels. Int Metals Rev 1979;20(5–6):205–30.
[6] Larsen JM, Worth BD, Annis CG, Haake FK. An assessment of the role of near-threshold crack growth in high-cycle-fatigue life prediction of aerospace titanium alloys under turbine engine spectra. Int J Fract 1996;80:237–55.
[7] Ritchie RO. Small cracks and high-cycle fatigue. In: Chang JCI, Coulter J, Brei D, Martinez WHG, Friedmann PP, editors. Proceedings of the ASME Aerospace Division. New York: ASM, 1996:321–33.
[8] Ritchie RO, Lankford J. Small fatigue cracks: a statement of the problem and potential solutions. Mater Sci Engng 1986;84:11–6.
[9] Döker H, Bachmann V, Marci G. A comparison of different methods of determining the threshold for fatigue crack propagation. In: Bäcklund J, Blom AF, Beevers CJ, editors. Fatigue thresholds, Proceedings of the 1st International Conference. Warley (UK): EMAS Lt, 1982:45–57.
[10] Herman WA, Hertzberg RW, Jaccard R. Influence of mean stress on fatigue in several aluminium alloys utilizing $K_{max}{}^c$ threshold procedures. Fat Fract Engng Mater Struct 1988;11:303–20.
[11] Pippan R, Plochl L, Klanner F, Stuwe HP. The use of fatigue specimens precracked in compression for measuring threshold values and crack growth. J Test Eval 1994;22(2):98–103.
[12] Aswath PB, Suresh S, Holm DK, Blom AF. Load interaction effects on compression fatigue crack growth in ductile solids. J Engng Mater Technol 1988;110(3):275–85.
[13] Eylon D. Summary of the available information on the processing of the Ti–6Al–4V HCF/LCF program plates. University of Dayton Report, Dayton (OH), 1998.
[14] Ritchie RO, Yu W. Short crack effects in fatigue: a consequence of crack tip shielding. In: Ritchie RO, Lankford J, editors. Small fatigue cracks. Warrendale (PA): TMS-AIME, 1986:167–89.
[15] Morgan JM, Milligan WW. A 1 kHz servohydraulic fatigue testing system. In: Soboyejo WO, Srivatsan TS, editors. High cycle fatigue of structural materials. Warrendale (PA): TMS, 1997:305–12.
[16] Coles A, Johnson RE, Popp HG. Utility of surface-flawed tensile bars in cyclic life studies. J Engng Mater Technol 1976;98:305–15.
[17] Newman JC Jr., Raju IS. An empirical stress-intensity factor equation for the surface crack. Engng Fract Mech 1981;15:185–92.
[18] Sarrazin C, Chiron R, Lesterlin S, Petit J. Electron backscattering pattern identification of surface morphology of fatigue cracks in TA6V. Fat Fract Engng Mater Struct 1994;17(12):1383–9.
[19] Halliday MD, Beevers CJ. Some aspects of fatigue crack closure in two contrasting titanium alloys. J Test Eval 1981;9(4):195–201.
[20] Ravichandran KS. Near threshold fatigue crack growth behavior of a titanium alloy: Ti–6Al–4V. Acta Metall Mater 1991;39(3):401–10.
[21] Ogawa T, Tokaji K, Ohya K. The effect of microstructure and fracture surface roughness on fatigue crack propagation in a Ti–6Al–4V alloy. Fat Fract Engng Mater Struct 1993;16(9):973–82.
[22] Dubey S, Soboyejo ABO, Soboyejo WO. An investigation of the effects of stress ratio and crack closure on the micromechanisms of fatigue crack growth in Ti–6Al–4V. Acta Mater 1997;45(7):2777–87.
[23] Schmidt RA, Paris PC. Threshold for fatigue crack propagation and effects of load ratio and frequency. In: Progress in fatigue crack growth and fracture testing. ASTM STP 536, 1973:79–94.
[24] Ritchie RO, Boyce BL, Campbell JP, Roder O. High cycle fatigue of turbine engine alloys. In: Proceedings of the 24th Symposium on Fatigue, Japan. The Society of Materials Science (Committee on Fatigue, 1998:1–6.
[25] Davidson DL. Southwest Research Institute, private communication, 1998.
[26] Morrissey RJ, McDowell DL, Nicholas T. Frequency and stress ratio effects in high cycle fatigue of Ti–6Al–4V. In: Stange WA, Henderson J, editors. Proceedings of the Third National Turbine Engine High Cycle Fatigue Conference (session 1, CD-ROM). Dayton (OH): Universal Technology Cor, 1998:21–30.
[27] Shih CF. Relationships between the *J*-integral and the crack opening displacement for stationary and extending cracks. J Mech Phys Solids 1981;29(4):305–26.
[28] Lütjering G, Hines JA, Peters JO. Technische Universität Hamburg-Harburg, private communication, 1998.
[29] Sadananda K, Shahinian PP. Prediction of threshold stress inten-

sity for fatigue crack growth using a dislocation model. Int J Fract 1977;13(5):585–94.
[30] Weertman J. Fatigue crack growth in ductile metals. In: Mura T, editor. Mechanics of fatigue. New York: ASME, 1982:11–9.
[31] Timothy SP, Hutchings IM. Influence of adiabatic shear bands on the fatigue strength of a titanium alloy. Fat Engng Mater Struct 1984;7(3):223–7.